This is pre-copyedit version of an article published in Journal of Cleaner Production.

The final authenticated version is available online at:
https://doi.org/10.1016/j.scitotenv.2019.07.009

Synthesis of super hydrophilic cellulose-alpha zirconium phosphate ion exchange membrane via surface coating for the removal of heavy metals from wastewater

Yazan Ibrahim [a], Elham Abdulkarem[a], Vincenzo Naddeo [b], Fawzi Banat [a], Shadi W. Hasan [a,*]

[a] Center for Membrane and Advanced Water Technology (CMAT), Department of Chemical Engineering, Khalifa University of Science and Technology, Masdar City Campus, P.O. Box 127788, Abu Dhabi, United Arab Emirates

[b] Department of Civil Engineering, University of Salerno, Via Giovanni Paolo II #132, 84084 Fisciano, SA, Italy

Highlights

•Cellulose/α-ZrP-n ion exchange membranes were fabricated via surface coating.
•Removal mechanisms of heavy metals were confirmed via membrane characterization.
•Up to 97, 98, and 99% removal of Cu (*II*), Zn (*II*), and Ni (*II*) were achieved.
•High water permeability through cellulose/α-ZrP-n membranes was accomplished.
•Cellulose/α-ZrP-n membranes reported slight improvement in tensile strength.

Abstract

In this study, commercial cellulose membranes were surface coated with alpha-zirconium phosphate nanoparticles (α-ZrP-n) to study their impact on the overall removal efficiency of heavy metals from synthetic metal mixture wastewater solution. A total of four homogeneous solutions (0.25, 0.50, 0.75, and 1.00 wt%) of α-ZrP-n were prepared by sonicating the nanoparticles in deionized water. These solutions were used to surface coat the commercial cellulose membranes. The Scanning Electron Microscopy (SEM) along with Energy Dispersive Spectroscopy (EDS) were used to confirm the attachment of α-ZrP-n on the cellulose membrane surface. Furthermore, the structural

characteristics of the *α*-ZrP-n modified cellulose membranes were also studied. The water contact angle results showed that all coated membranes remained super-hydrophilic. The porosity of the membranes decreased to 48% with the addition of 1.00 wt% *α*-ZrP-n compared to 65% for the pristine membrane. The mechanical strength has improved from 3.4 MPa for the pristine membrane to about 4 MPa for the 1.00 wt% *α*-ZrP-n membrane. Similarly, the thermal stability was found to be slightly enhanced as evidenced by the increase in decomposition temperature to 280 and 285 °C in the 0.75 and 1.00 wt% *α*-ZrP-n membranes, respectively. Furthermore, a removal efficiency of 97.0 ± 0.6, 98.0 ± 0.5, 99.5 ± 0.2, and 91.5 ± 2.0% for Cu (*II*), Zn (*II*), Ni (*II*), and Pb (*II*), respectively, was observed with the 0.50 wt% *α*-ZrP-n membrane. This removal was achieved at a flux of 41.85 ± 0.87 × 10^3LMH. Increasing the *α*-ZrP-n concentration further did not show any improvement in the overall removal efficiency. However, it led to 46% flux reduction in the 1.00 wt% *α*-ZrP-n membrane. The mechanism of removal of the heavy metal ions was postulated to be a combination of ion exchange and electrostatic attraction of the strong negatively charged *α*-ZrP-n membranes and the free metal ions in the wastewater solution.

Graphical abstract

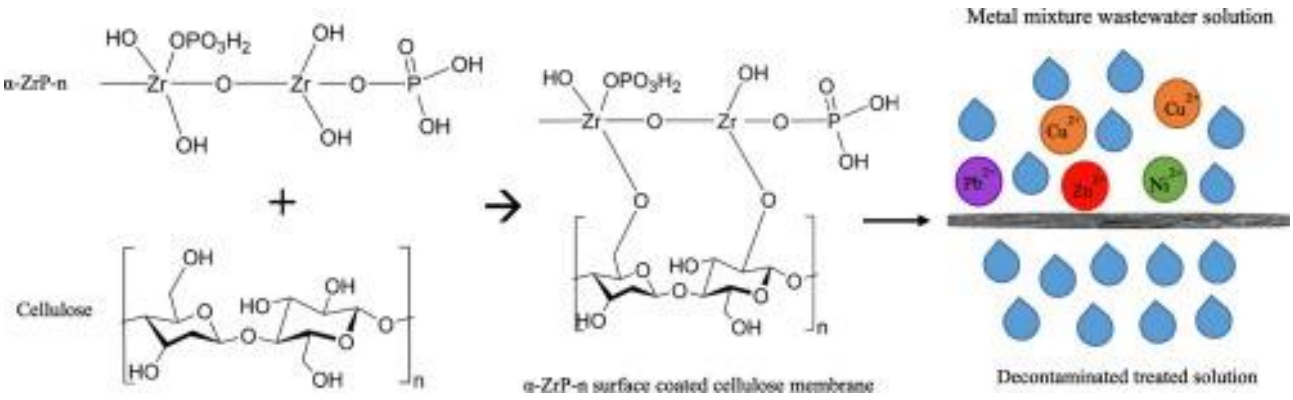

Keywords

Cellulose membranes
Zirconium phosphate
Surface coating
Wastewater
Heavy metals

1. Introduction

Recently, freshwater resources have been decreasing across the globe due to climate change (Benateau et al., 2019), contamination (Schwartz and Ibaraki, 2011), and industrial and population growth (Vörösmarty et al., 2000). This has contributed to the spread of water scarcityworldwide (Steduto et al., 2017). Wastewater reuse is one of the feasible approaches to reduce this scarcity and increase the amount of clean water supply (van Loosdrecht and Brdjanovic, 2014). Nonetheless, the treated volumes of wastewater may still contain trace amounts of several contaminants that are harmful to humans and the environment. Heavy metals such as Zn (*II*), Cu (*II*), Ni (*II*), and Pb (*II*) are found commonly in sewage effluents and pose a serious health threat to humans even at a very low concentration (Ahmed and Hasan, 2017; Ali et al., 2019; Giwa et al., 2018). For example, Cu (*II*) leads to liver, kidney, and nervous system damage (Mohod and Dhote, 2013; US EPA, 2009) when the body is exposed to >2 mg/L (World Health Organization, 2004). Similarly, long exposure to Ni (*II*) at a concentration higher than 0.07 mg/L causes cell damage and cancer (Mohod and Dhote, 2013; World Health Organization, 2004; Zambelli et al., 2016).

There are several methods used for the removal of heavy metals including adsorption, chemical precipitation, electrochemical processes, ion exchange, membrane separation, etc. (Fu and Wang, 2011). In addition, the heavy metal detection plays an important role in the removal of these metal ions from wastewater effluents (Rasheed et al., 2018). Membrane technologies show tremendous potential in heavy metal removal from wastewater effluents (Bolisetty et al., 2019; Nabeel et al., 2019). These technologies are known for high removal efficiencies, low environmental impacts, reduced land use, and ease of operation (Basile et al., 2015; Ibrahim et al., 2018). Microfiltration (MF), which operates at very low pressure and with relatively high water flux, is an example of membrane-based technologies used in heavy metals removal. Typically, MF membranes (with a pore size between 0.1 and 10 μm) are used for particle separation from a solution (Huisman, 2000). These membranes can be made from cellulose, which is one of the most abundant resources of polymers worldwide. Cellulose possesses versatile properties and is relatively cheap compared to other resources (Bhattacharyya et al., 1998). These membranes have reactive hydroxyl groups which can bond with heavy metal ions via ion-exchange or adsorption mechanism (Kamel et al., 2006). For example, cellulose/poly (vinyl alcohol) (PVA) composite membranes were fabricated and tested for the removal of Cu (*II)* from aqueous solution (Çifci and Kaya, 2010). Removal efficiency of around 45% (pH = 7) was achieved for Cu (*II)* in the composite membrane compared to a negligible removal in the pristine cellulose membrane. Similarly, pure cellulose membranes were chemically modified

with ethylenediaminetetraacetic acid (EDTA) and used for the remediation of Pb (*II*) from metal-containing water sample (D'Halluin et al., 2017). Removal efficiency of around 90% was archived via the cellulose-EDTA membrane compared to <20% in the pure cellulose membrane. Cellulose MF membranes cannot be used alone for the removal of heavy metals due to the limited ion-exchange and adsorption capacity of the membrane's surface area (Bhattacharyya et al., 1998). In order to enhance the adsorption capacity of the membranes, incorporation of nanoparticles (nano-adsorbent) on the membrane's surface can be used (Ritchie et al., 1999). This allows for the creation of several ion binding sites on the membrane's surface which would significantly enhance the capture capacity of the heavy metals and their removal. There is a wide range of micro/nano particles that can be used for this purpose. These include, but are not limited to, activated carbon (d = 45.5 μm), carbon nanotubes (d = 20 nm), kaolinite (d = 66.5 μm), zeolites (d = 38.5 μm), aragonite shells (d = 32.5 μm), cetyltrimetylammoniumbromide, 8-Hydroxyquinoline, and others (Apiratikul and Pavasant, 2008; Daniş and Keskinler, 2009; Fu and Wang, 2011; Jiang et al., 2010; Kabbashi et al., 2009; Köhler et al., 2007; Kongsuwan et al., 2009; Li et al., 2010; Madaeni and Heidary, 2012; Wang et al., 2007). Table S1 shows some examples of nanoparticles used with MF membranes for the removal of certain heavy metals from wastewater effluent.

More recently, alpha-zirconium phosphate nanoparticles (α-Zr-n) has been used with graphene oxide (GO) to remove Pb (*II*), Cd (*II*), Cu (*II*), and Zn (*II*) from a synthetic wastewater sample (Pourbeyram, 2016). These nanoparticles are known to be a nontoxic metal cation with a high ionic and coordinative affinity for O_2 containing groups. In addition, it has high catalyst activities and significant adsorptive capabilities (Cai et al., 2012; Karlsson et al., 2001; Xiao and Liu, 2018). Studies related to the incorporation of α-ZrP-n into polymer membranes for removal of heavy metals are limited. Abutartour et al. (2014) fabricated porous membrane made of SiF_4 and hexadecyl trimethyl ammonium bromide. Zirconium in the form of $ZrOCl_2 \cdot 8H_2O$ was added to the membrane matrix by which the membrane showed improved removal for both Cu (*II*) and Pb (*II*). Hollow fiber membranes (HFM) made of polysulfone (PSF) and zirconium oxychloride were synthesized and tested for the removal of arsenate (He et al., 2014). The membranes showed enhanced removal of arsenate from the aqueous solution. Zhao et al. (2016) fabricated hydrophobic PVDF membranes and modified them with PVA/ZrP for the removal of lead (*II*). The optimal lead (*II*) adsorption was achieved at a pH of 5.5. Zhang et al. (2017) prepared a composite membrane made of zirconium-chitosan and GO for the removal of fluoride. Results revealed high removal

over a wide range of pH ranging between 3 and 11. To the best of our knowledge, no attempts on fabricating cellulose membranes incorporating α-ZrP-n were reported in the literature, neither via phase inversion and surface coating nor by other fabrication methods. Therefore, the main objective of this research study was to synthesize α-ZrP-n surface coated cellulose membranes for the removal of heavy metals from wastewater. Several membrane characterizations and performance tests were carried out and the results are explained in the subsequent sections.

2. Materials and methods

2.1. Materials

Commercial pure cellulose membranes with a pore size of 7–9 μm and a thickness of 170 μm were provided by Filtros Anoia, SA. Galwick™ was purchased from Porous Materials, Inc. and was used as a wetting liquid. Nano-sized α-ZrP-n, having an average particle size diameter of 100 nm, were provided by Guizhou Zerophos Chemical Co., Ltd. (China). Deionized water (DI) with a resistivity of 17 MΩ·cm at 23 °C was used for the dispersion of α-ZrP-n and for the cleaning of any excess nanoparticles after the surface coating. HACH detection cuvettes (LCK 337, LCK 306, LCK 360, LCK 364, and LCK 329) were used to measure the concentration of heavy metals in wastewater and treated filtrate using HACH DR3900 UV/Vis spectrophotometer with radio-frequency identification (RFID) technology. The pH measurements on all samples were carried out using a HACH HQ40D probe.

2.2. Surface coating of cellulose membranes with α-ZrP-n

Analytical grade α-ZrP-n were dispersed in water with concentrations of 0.25, 0.50, 0.75 and 1.00 wt%. The use of relatively low weight concentrations was to avoid agglomeration and ensure uniform dispersion of the nanoparticles in DI water. All four solutions with nanoparticles were sonicated using Branson® Ultrasonic Bath (5510 B-series) for 2 h to ensure better dispersion and homogeneity. Furthermore, the sonicated mixtures were continuously stirred at 250 rpm by a magnetic stirrer for 2 h in order to ensure maximum homogeneity. The solution mixtures were immediately sprayed onto the surface of the pure cellulose membranes under vacuum filtration using WELCH 2546C-02A vacuum pump (Gardner Denver Thomas, Inc.). The obtained membranes were then dried in the Memmert UF55 oven at 60 °C for 3 h and thermally treated at 90 °C for 4 h. The dried membranes were then washed with DI water thrice to remove

any excess α-ZrP-n. The membranes were then dried and stored in a sealed container at room temperature. Fig. 1 illustrates the fabrication of cellulose α-ZrP-n coated membranes via a surface coating method.

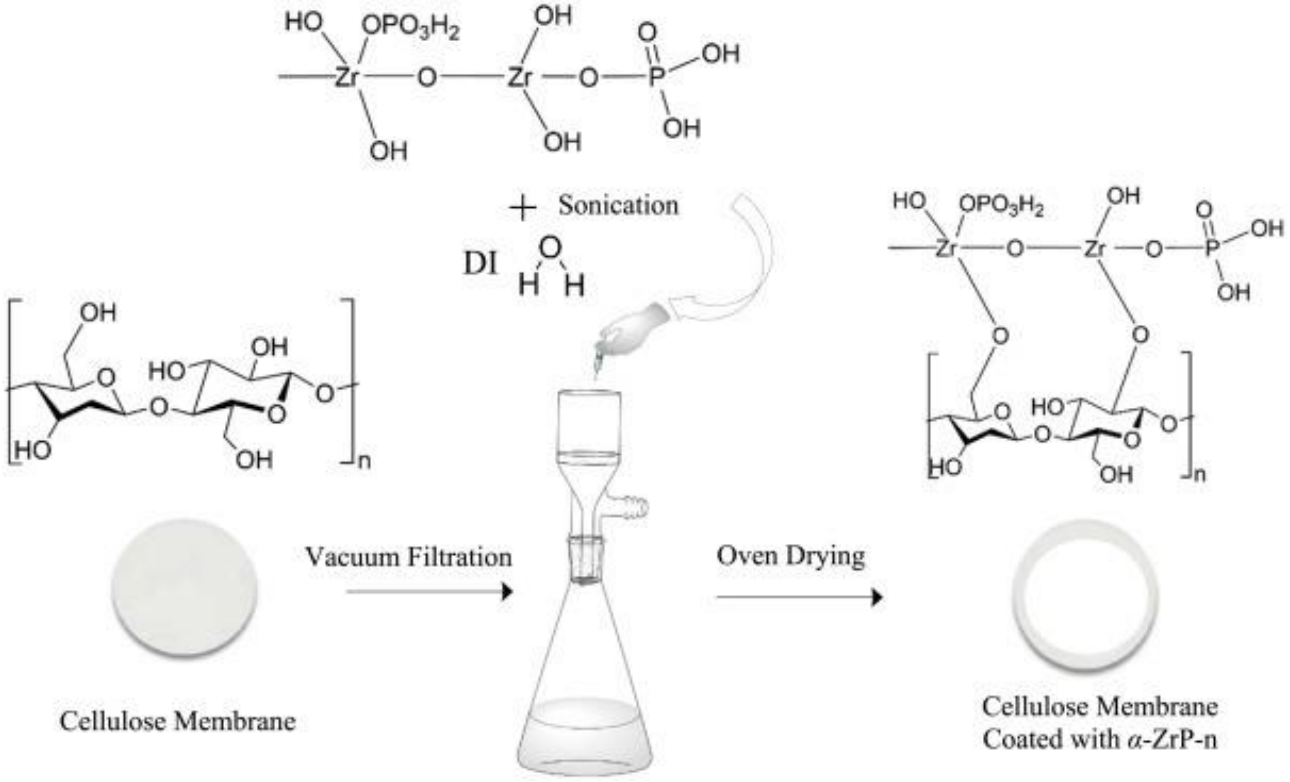

Fig. 1. Schematic representation of the fabrication of the cellulose α-ZrP-n coated membranes via surface coating.

The surface-coated membranes with 0.25, 0.50, 0.75, and 1.00 wt% of α-ZrP-n were named as ZrP-C1, ZrP-C2, ZrP-C3, and ZrP-C4, respectively. The pristine commercial cellulose membrane was denoted as C and used as a reference membrane for comparison. To investigate α-ZrP-n leaching into filtered water, coated membranes were immersed in DI water for 12 h to verify the degree of attachment of the α-ZrP-n to the cellulose membrane surfaces. The DI water was then tested for the presence of zirconium using HACH DR3900 UV/Vis spectrophotometer with radio-frequency identification (RFID) at a wavelength of 500 nm.

2.3. Characterization of pristine and cellulose α-ZrP-n coated membranes

The surface morphology including cross-sectional structure and surface shape of the pristine and coated membranes was observed using Quanta250 Scanning Electron Microscope (SEM). Liquid nitrogen was used to prepare the samples for the cross-sectional analysis by freeze-fracturing technique. Since the membranes were made of pure non-conductive cellulose, all membranes were first coated with 100 Å gold layer. The presence of α-ZrP-n was confirmed using Energy Dispersive X-ray Spectroscopy

(EDS) at an accelerating voltage of 1.6 keV (scanning area of 5 × 5 μm^2). To further confirm the attachment of α-ZrP-n on the membrane's surface, X-ray Diffraction (XRD) analysis was carried out on these samples using PANalytical Empyrean (40 kV and 35 mA). Fourier Transform Infrared (FT-IR) spectroscopy was used to study the functionalities in the cellulose fibers in both the pristine and surface coated membranes. The IR attenuated total reflectance (ATR) spectra analysis using Bruker's Vertex 80v FT-IR spectrometer was performed in the wavelength range of 4000 to 400 cm^{-1} and a resolution of 4 cm^{-1}. The mechanical stability of the membrane including tensile strength and elongation was investigated using the INSTRON's Blue Hill device (Canada). Membranes were cut into strips of 65 × 10 mm (length × width) on both ends, and 20 × 5 mm^2in the middle. The ends were fixed between grips such that only the 20 × 5 mm^2 area was exposed to the load. The maximum tensile strength in MPa was recorded for all the membranes samples using a crosshead speed of 0.05 mm/min. Furthermore, contact angle measurements of each sample were obtained from Krüss GmbH' Drop Shape Analyzer (DSA) by using 2 µL DI water droplets. A thermogravimetric analyzer (PerkinElmer, TGA 4000) was used to determine the thermal stability of each membrane. The membranes were heated to a temperature of 700 °C in O_2 environment at a heating rate of 10 °C/min. Weight loss due to thermal decomposition was recorded and used to study the membranes' thermal stability. The gravimetric method was used to evaluate the porosity of all membranes used in this work. First, dry membrane samples with a total area of 1 cm^2 and 170 µm thickness were wetted with Galwick™ in order to fill all the membrane pores. Then, the ratio of the wetted pores volume to the total membrane volume was used to calculate the porosity. The nanoparticles surface charge at different pH values was also measured using ZetaPALS (Brookhaven Instrument). The α-ZrP-n were added to DI water (concentration of 0.2 mg/mL) and sonicated for 1 h to ensure maximum homogeneity. In order to adjust the pH of the solution, both HCL and NaOH were used at concentrations of 100 mM. The cellulose membrane surface charge was measured using Anton Paar SurPASS Electrokinetic Analyzer (USA). Two membrane samples (10 × 20 mm (W × L) each) were placed in an adjustable clamping cell and separated by a spacer that allowed for electrolyte flow. Three solutes were used in this process, 1 mM KCl, 50 mM HCl, and 50 mM NaOH.

2.4. Preparation of synthetic metal mixture wastewater solution and water quality analysis

Synthetic metal mixture wastewater solution was prepared by dissolving copper nitrate ($Cu(NO_3)_2 \cdot 3H_2O$), nickel chloride ($NiCl_2 \cdot 6H_2O$), zinc chloride ($ZnCl_2$), and lead nitrate $Pb(NO_3)_2$ in 5 L of DI water. The weights added to the DI were calculated such that the final Cu (*II*), Ni (*II*), Zn (*II*), and Pb (*II*) concentrations were 8.4 ± 0.2, 5.5 ± 0.1, 5.5 ± 0.3, and 5.4 ± 0.5 mg/L, respectively. The synthesized solution sample was then characterized using LCK HACH vials using HACH DR3900 UV/Vis spectrophotometer with radio-frequency identification (RFID) at wavelengths of 478, 466, 466, and 520 nm for Cu (*II*), Ni (*II*), Zn (*II*), and Pb (*II*), respectively. The removal efficiency of heavy metals was calculated using Eq. (1):

$$Removal\ (\%) = \left(\frac{C_F - C_P}{C_F}\right) \qquad (1)$$

where C_F and C_P are the heavy metal concentrations (in mg/L) in the feed and permeate, respectively.

2.5. Performance tests of pristine and cellulose α-ZrP-n coated membranes

Several vacuum filtration experiments using pristine and cellulose α-ZrP-n coated membranes were carried out to investigate the impact of α-ZrP-n on water flux, permeability, and permeate quality. The filtration setup used in this study consisted of a PALL 4241-DS funnel magnetic filter setup installed on a glass flask and connected to the WELCH 2546C-20A vacuum pump. Water permeability and flux were calculated using Eqs. (2), (3), respectively:

$$Pure\ Water\ Permeability = \frac{V}{A \times t \times P} \quad (2)$$

$$Pure\ Water\ Flux = \frac{V}{A \times t} \quad (3)$$

where V is the permeate volume in L, A is the membrane's effective surface area in m^2, t is the time needed to collect the permeate in h, and P is the pressure applied to the membrane in bar.

3. Results and discussion

3.1. Characterization of pristine and cellulose α-ZrP-n coated membranes

3.1.1. α-ZrP-n interaction with cellulose membrane and leaching effects

Fig. S1 shows the possible interaction between α-ZrP-n and the cellulose membrane. Drying the surface coated cellulose membranes with α-ZrP-n at 90 °C resulted in water

evaporation which led to a covalent attachment of α-ZrP-n to the cellulose membrane, as illustrated schematically in Fig. S1.

In order to investigate the degree of attachment of α-ZrP-n, leaching experiment was carried out on the coated membranes by submerging the membranes in DI water for 24 h. Results showed no presence of zirconium in the tested water sample (using HACH DR3900 spectrophotometer) confirming the strong attachment of the α-ZrP-n on the coated cellulose membranes.

3.1.2. XRD and FT-IR analyses

In order to confirm the presence of α-ZrP-n on the surface of the membrane, XRD analysis was performed and the results are shown in Fig. 2(a). The broad peaks B and D are the unique characteristics peaks of the cellulose fibers which also show the degree of crystallinity of those fibers (Zhao et al., 2007). In addition, the XRD pattern showed five characteristic peaks A, C, E, F, and G of crystalline α-ZrP-n at $2\theta = 12.5$, 20.1, 25.4, 27.5, and 34.5°, respectively (Sun et al., 2007; Wu et al., 2010). The first three correspond to d (002), d (110), and d (112) (Han et al., 2018). The exclusive d (002) peak corresponded to the crystal plane of α-ZrP-n.

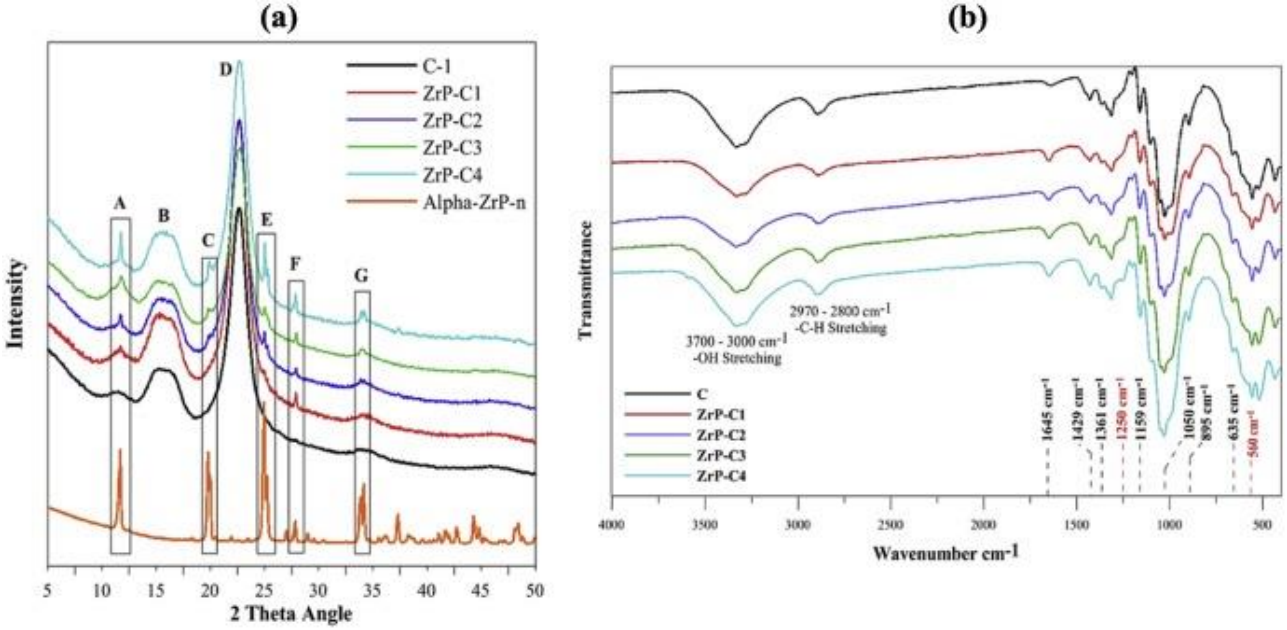

Fig. 2. (a) XRD, and (b) FT-IR analyses of the pristine and α-ZrP-n coated membranes.

The IR spectra of the pristine cellulose membrane and the α-ZrP-n coated membranes are shown in Fig. 2(b). The broad peak at 3000–3700 cm^{-1} could be attributed to asymmetric and symmetric –OH stretching (Patel and Chudasama, 2007). The peak at 2800–2970 cm^{-1} is related to the –C-H stretching where peak intensity is usually used to determine the organic material content of the cellulose fibers (Garside and Wyeth,

2003). The sharp and relatively small peak at 1645 cm^{-1}could be ascribed to the (H-O-H) bending (Garside and Wyeth, 2003). The peaks at 1429, 1361, and 1159 cm^{-1} belong to the symmetric bending of $–CH_2$, bending of C—H, and vibration of C-O-C, respectively (Barud et al., 2008, Barud et al., 2011). The CO stretching peak is observed at 1050 cm^{-1}, whereas the C-OH peak is observed at 1023 cm^{-1}. In addition, the 1034 cm^{-1} peak is related to the C—C stretching, and the 895 cm-^{1} peak corresponds to the symmetric in plane C-O-C stretching (Garside and Wyeth, 2003; Oh et al., 2005). An out-of-phase bending peak of OH is noticed at 635 cm^{-1}. These peaks are a unique characteristic of cellulose membranes. On the other hand, the peak at 1250 cm^{-1} is due to the bending vibration of P-OH (Han et al., 2018). This peak is only visible in the IR spectra of the ZrP-C4 which has the highest zirconium phosphate content. The orthophosphategroups stretching peak in the range of 1000–1200 cm^{-1} is overlapped by the cellulose unique characteristic peaks. Similarly, the P═O stretching peak at 1034 cm^{-1} indicates a possible overlapping stretching of the C—C bond (Patel and Chudasama, 2007). Finally, the Zr—O extending vibration peak at 560 cm^{-1} (Huang et al., 2017) is visible in ZrP-C1, ZrP-C2, ZrP-C3, and ZrP-C4.

3.1.3. Surface/cross-sectional morphology and EDS analyses

In order to investigate the structure of the cellulose membrane and α-ZrP-n attachment, SEM images and EDS analysis of surface coated membranes were captured and are shown in Fig. 3. All membranes showed clear, smooth, and dense fibers without the presence of any noticeable trenches. The macro fibers diameters were in the range of 10–20 μm and are well separated and followed a rod-shaped structure. The attached α-ZrP-n on the ZrP-C1 membrane could be observed in Fig. 3(b). The nanoparticles are possibly attached on the cellulose fibers as a result of the strong covalent bond between the cellulose membrane and the α-ZrP-n, as explained earlier in Section 3.1.1 (He et al., 2003; Maneerung et al., 2008). The presence of the nanoparticles on the cellulose membrane fibers increased as the α-ZrP-n concentration increased (Fig. 3(c), (d), and (e)). It was also observed that the α-ZrP-n had slightly encapsulated the cellulose fibers in ZrP-C4 membrane which might lead to moderate agglomeration of the α-ZrP-n as a result of the van der Waals forces between the nanoparticles (Danilenko et al., 2012; Feng et al., 2007).

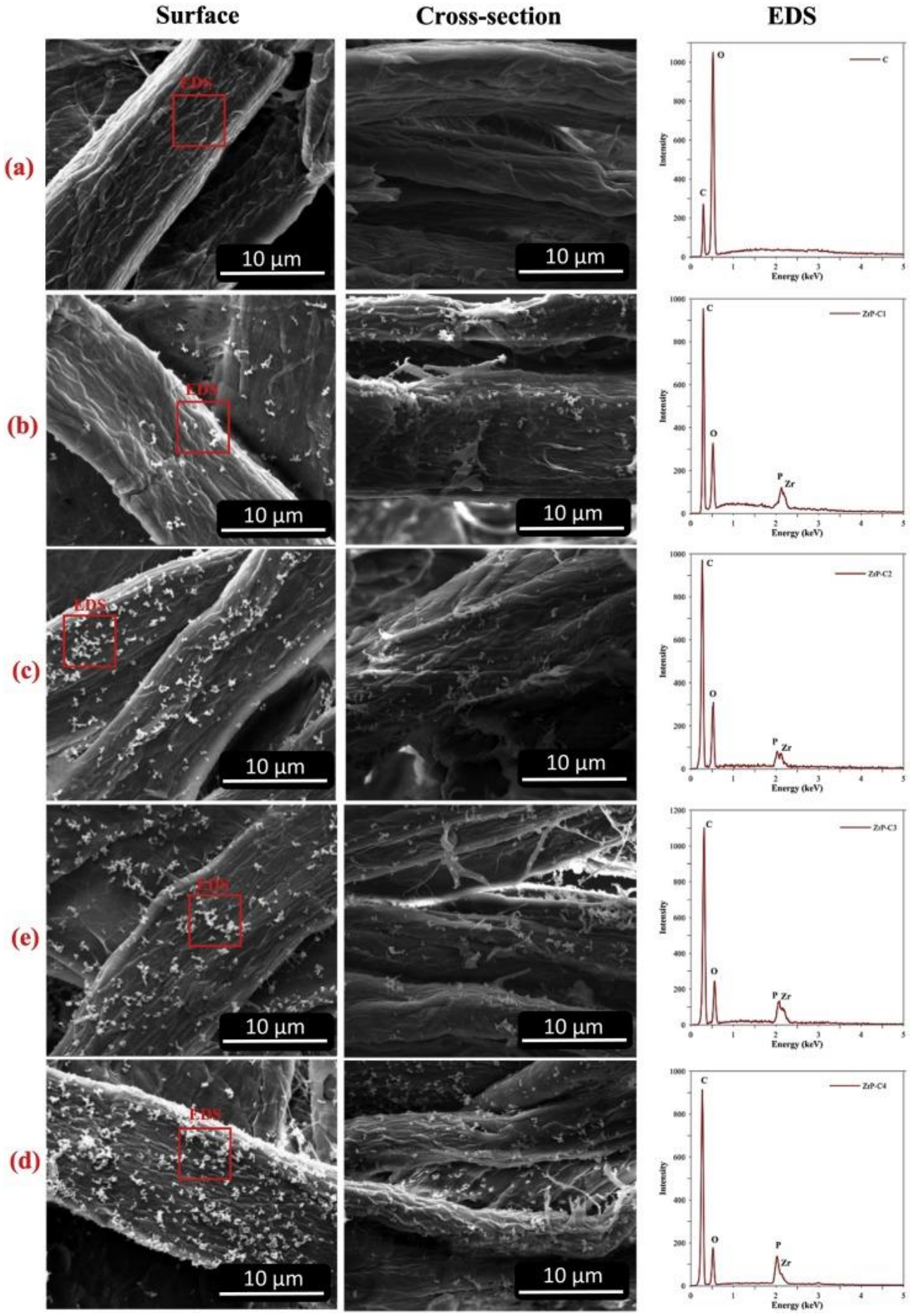
Surface
Cross-section
EDS
(a)
(b)
(c)
(e)
(d)
EDS
10 μm
C
O
P
Zr
Intensity
Energy (keV)
ZrP-C1
ZrP-C2
ZrP-C3
ZrP-C4

Fig. 3. Surface, cross-sectional and EDS analysis of the membranes showing the cellulose fibers coated with α-ZrP-n: (a) C, (b) ZrP-C1, (c) ZrP-C2, (d) ZrP-C3, and (e) ZrP-C4.

Cellulose membranes are usually made up of an interconnected non-woven 3D network of fibers that could facilitate the penetration of α-ZrP-n throughout the inner space of the fibers network via the pores formed between the fibers (Wu et al., 2014). This could be observed from the SEM cross-sectional images shown in Fig. 3. The α-ZrP-n could be clearly seen attached to the inner macro cellulose fibers.

The presence of unique characteristic peaks of the crystalline α-ZrP-n shown in Fig. 2(a) (XRD results) were in line with the morphological and cross-sectional SEM imaging (Fig. 3) which confirmed the existence and attachment of the α-ZrP-n onto the membrane's surface and sub-surface.

The EDS analysis was carried out to identify the elemental structure of the pristine and coated cellulose membranes. The EDS spectrum of the C membrane (Fig. 3(a)) showed only two sharp peaks of both carbon (C) and oxygen (O_2) which are a cellulose elemental structure (Fig. 1). On the other hand, the EDS results of ZrP-C1, ZrP-C2, ZrP-C3, and ZrP-C4 membranes shown in Fig. 3(b), (c), (d), and (e) respectively, exhibited a unique and moderately intense characteristic peaks of both zirconium and phosphate at Lα = 2.042 keV and Kα = 2.013 keV, respectively. This, along with SEM and XRD analyses, confirmed the presence and attachment of α-ZrP-n onto the cellulose membrane. The change in the intensity of the carbon peaks (Fig. 3(a) and (b)) was likely due to the unpredictability of EDS in detecting carbon (Arepalli et al., 2004). This could be due to the weak sensitivity of the EDS detector when it comes to low energy spectrums where carbon is located (Kα = 0.277 keV) (Arepalli et al., 2004).

3.1.4. Mechanical and thermal stability

The α-ZrP-n coated membranes showed a slight improvement in the tensile strength as shown in Fig. 4(a). The average tensile strength of the cellulose membranes increased from 3.4 MPa to 4 MPa in the α-ZrP-n coated ones (Fig. 4(a)). The minor enhancement in the tensile strength could be related to the possible interfacial interaction between the α-ZrP-n and the cellulose fibers (Wu et al., 2010). In membrane composites, interfacial interaction between fillers (α-ZrP-n) and the membrane fibers is a critical factor that affects the tensile strength (Mansour et al., 2018; Wu et al., 2010). Initially, no change in the tensile strength was observed in the ZrP-C1 membrane which is mostly due to the low concentration of the α-ZrP-n. However, with the increase of ZrP concentration, the mechanical strength of the cellulose membranes has marginally

increased reaching 4 MPa in the ZrP-C4. This confirms the stress transfer from the cellulose fibers to the incorporated α-ZrP-n. On the other hand, the tensile strain (elongation) of the surface coated membranes has decreased significantly from 1.27% in the C to around 0.38% in ZrP-C1. Nonetheless, with the increase of α-ZrP-n, the drop in ductilitybecomes less significant. The cellulose fibers lose part of their ductility as a result of the possible defects formed after the α-ZrP-n impregnation (Mulinari et al., 2009). The tensile properties are highly depended on the microstructural distribution of the nanoparticles on the membrane's surface (Mulinari et al., 2009).

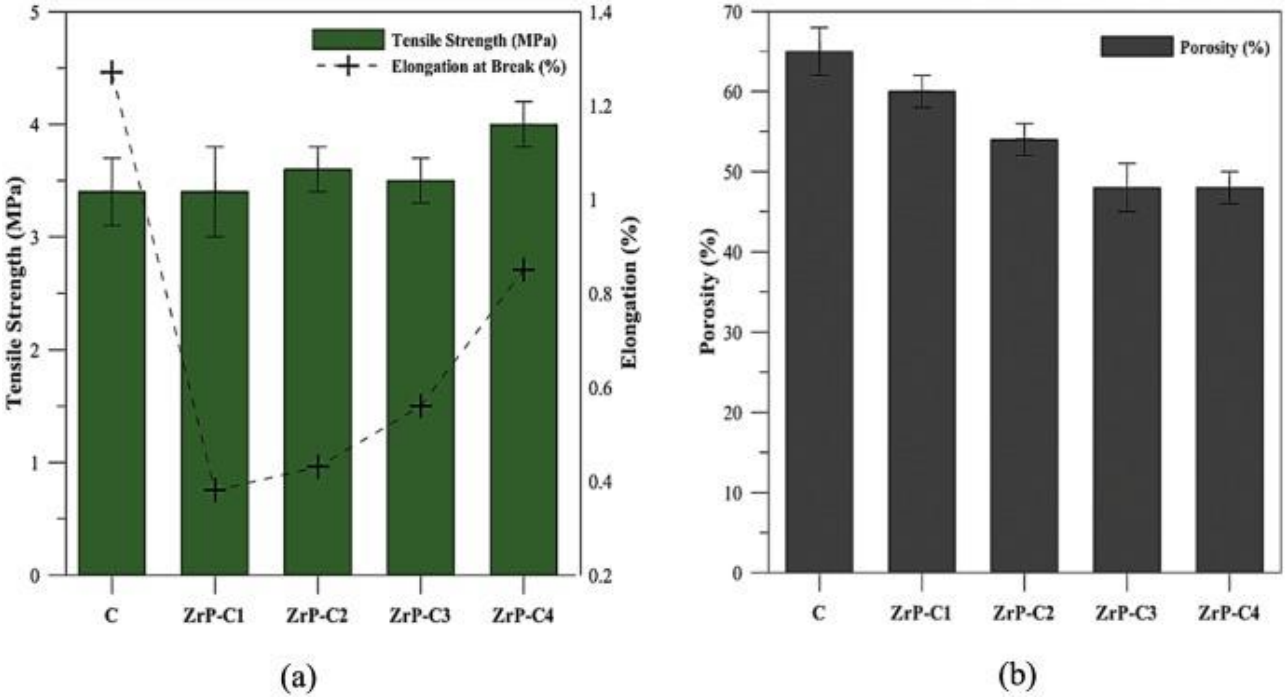

Fig. 4. Impact of adding the α-ZrP-n to the cellulose membranes: (a) Mechanical stability, and (b) Porosity (The error bars denote standard deviations which were calculated using three measurements).

The trend observed in Fig. 4(b) clearly depicts the reduction in membrane's porosity with an increase in α-ZrP-n concentration. As a result of the nano-filling of the membrane's pores, a reduction in the average porosity could be observed from ca. 65% in the pristine cellulose membrane to about 60, 54, and 48% for 0.25, 0.50, and 0.75 wt% α-ZrP-n impregnated membranes, respectively. No further reduction in porosity was observed with the continued increase of the nanoparticles concentration (i.e. at 1.00 wt% α-ZrP-n the porosity was 48%). The above finding, therefore, indicates that most of the cellulose fibers and pores were occupied at 0.75 wt% of α-ZrP-n.

The thermal stability of the membranes was investigated through the thermogravimetric analysis and the results are shown in Fig. S2. Initially, all membranes exhibit a weight loss at a temperature below 100 °C which is related to the moisture in both the cellulose

fibers and nanoparticles. The pristine cellulose membrane showed two decomposition phases: 1) at 270 °C where the membrane starts to degrade, and 2) at around 500 °C which corresponds to the complete decomposition of the membrane.

The decomposition temperature of both ZrP-C1 and ZrP-C2 membranes were similar to the pristine cellulose (around 270 °C) indicating that small concentrations of the α-ZrP-n are not likely to increase the thermal stability of the membrane. On the other hand, a slight increase in the decomposition temperature of both ZrP-C3 and ZrP-C4 relative to the pristine cellulose membrane was observed (Fig. S2). The ZrP-C3 membrane started to decompose at 280 °C whereas ZrP-C4 decomposition temperature was around 285 °C. This improvement could be related to the strong bonding characteristics between the α-ZrP-n the cellulose fibers (Raghavendra et al., 2013).

Thermogravimetric results summarized in Table 1 include the percentage of mass loss in each respective range of temperature. The data shows that both ZrP-C1 and ZrP-C2 have a similar mass loss in the 200–500 °C range when compared to the pristine cellulose membrane. However, both ZrP-C3 and ZrP-C4 membranes exhibited a lower mass loss of 77.4 and 71%, respectively in the same temperature range. The percentage of residue increased in the coated membranes due to the presence of oxides on the membrane's surface (Mulinari et al., 2009).

Table 1. Results of the thermogravimetric analysis curves with the % of mass loss, temperature range, and total residue.

Membrane	**Mass loss (%)**	**ΔT (°C)**	**Residue (%)**
C	6.8	22–200	1.1
	83.3	200–500	
	8.8	500–700	
ZrP–C1	5.4	22–200	6.9
	84.6	200–500	
	3.1	500–700	
ZrP–C2	5.3	22–200	5.7
	85.6	200–500	
	3.4	500–700	
ZrP–C3	3.0	22–200	15.7
	77.4	200–500	
	3.9	500–700	
ZrP–C4	1.2	22–200	21.8
	71.2	200–500	
	5.7	500–700	

3.1.5. Water contact angle, flux, and permeability

The contact angle measurements of the pristine and α-ZrP-n membranes showed a complete wetting of the membranes. A receding contact angle of 0° was observed for all the membranes (both pristine and *α*-ZrP-n coated). This value was recorded with a span of 1 s after the contact of the membrane's surface with the water drop as shown in Fig. 5(b) (similar behavior was observed for all *α*-ZrP-n coated membranes). This super hydrophilicity led to significantly high water flux as shown in Fig. 5(a).

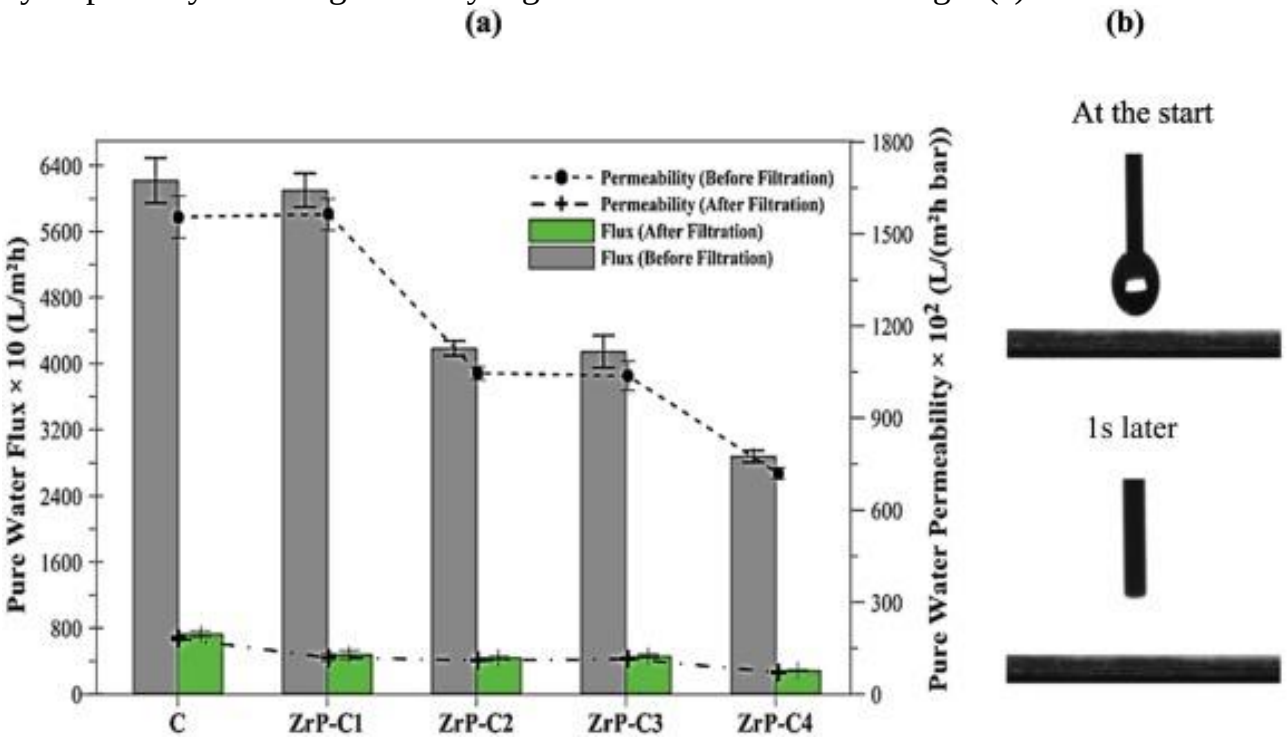

Fig. 5. (a) Pure water flux and permeability of the pristine cellulose and *α*-ZrP-n coated membranes (before and after the wastewater filtration) (The error bars denote standard deviations which were calculated using three measurements) (b) The contact angle of the pristine and surface coated cellulose membrane.

Additionally, the pure water flux of ZrP-C1 showed a slight decrease when compared with the water flux obtained using the C membrane. However, with further increase in the *α*-ZrP-n concentration (e.g. ZrP-C2, ZrP-C3, and ZrP-C4), the water flux significantly reduced to ca. 54% in ZrP-C4. The flux data were in line with the membrane porosity results that showed a noticeable decrease in the average membrane's porosity with the increase of the *α*-ZrP-n coating (Fig. 4(b)) (Saljoughi et al., 2009).

3.1.6. Surface charge and zeta potential measurements

One of the very important surface properties of membranes in water applications is the surface charge. This can be evaluated by determining the zeta potential of the membrane

surface. In this work, the zeta potential of both the pristine cellulose and *α*-ZrP-n was measured and the results are illustrated in Fig. 6. The pristine cellulose membrane's surface exhibited a positive charge at pH < 5 (Fig. 6(a)). At neutral conditions (pH = 7), the membrane's surface charge was found to be around −21.75 mV. Any further increase in the pH value resulted in a further reduction in the membrane's surface charge reaching around −30.5 mV at pH = 11 (Fig. 6(a)). The negatively charged OH^- groups and the adsorbed anions in the cellulose structure leads to such negative values (Mohan et al., 2011). The isoelectric point at which the OH^- groups were protonated was found to be around a pH of 5. The results are comparable to values found in the literature for the pristine cellulose membranes (Ristić et al., 2014). Also, the *α*-ZrP-n showed a very strong negative surface charge as can be clearly seen from Fig. 6(b). The isoelectric point (deprotonation) occurs approximately at pH = 3.1. From this point, the zeta potential value decreased significantly to around −47 mV at pH ~12. Similar results have been reported in the literature (Chalkova et al., 2007; Su et al., 2013).

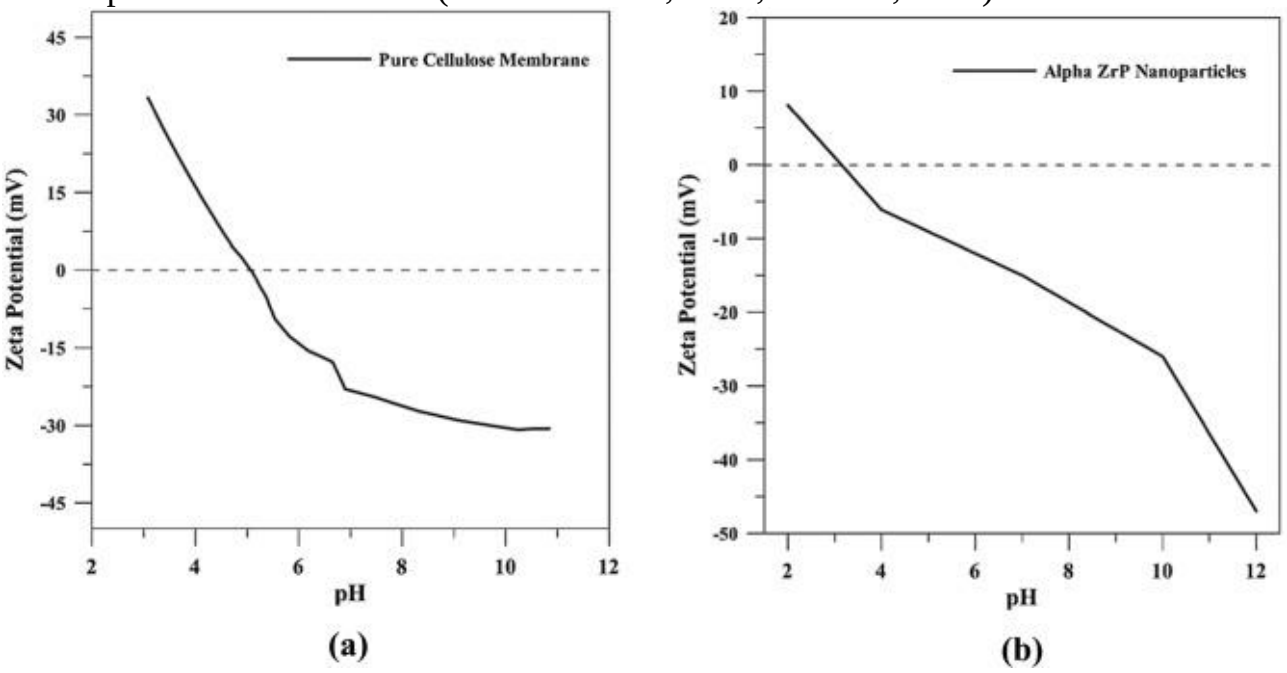

Fig. 6. Zeta potential measurements of both: (a) pristine cellulose, and (b) *α*-ZrP-n.

3.2. Performance tests and water quality analyses of pristine and cellulose α-ZrP coated membranes

The synthetic wastewater sample containing heavy metals was filtered using both the pristine cellulose and *α*-ZrP-n coated membranes using vacuum filtration. The removal efficiency was calculated using Eq. (1)and the results are shown in Fig. 7. Results showed that impregnating *α*-ZrP-n on the cellulose membrane surface has improved the

removal of heavy metals at neutral conditions (i.e. pH = 7). The stoichiometric ion exchange equation of the metal ions onto the *α*-ZrP-n is explained in Eq. (4):

$$Zr(HPO_4)_2 \cdot H_2O + 0.5M^{2+} \rightleftharpoons ZrM_{0.5}H(PO_4)_2 \cdot H_2O + H^+ \quad (4)$$

where M is the heavy metal element.

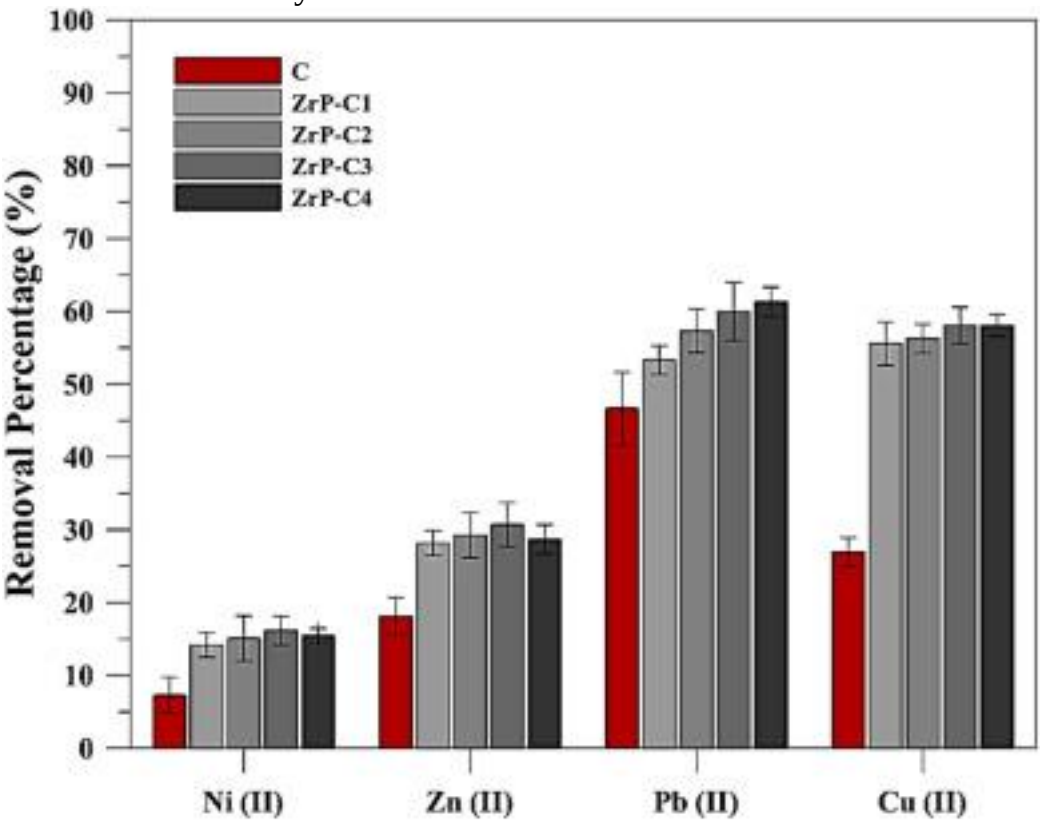

Fig. 7. The overall removal efficiency of the pristine cellulose and *α*-ZrP-n coated membranes at pH = 7 (The error bars denote standard deviations which were calculated using three measurements).

Ni (*II*) removal percentage doubled when α-ZrP-n coated membranes were employed in place of pristine cellulose (Fig. 7). In an aqueous solution containing a 10^{-4} M $NiCl_2$ (the case here), the dominant nickel species is in the form of Ni (*II*) (Ji and Cooper, 1996). Therefore, the observed increase in Ni (*II*) removal percentage can be attributed to the electrostatic attraction between the Ni (*II*) and the $Zr(HPO_4)_2 \cdot H_2O$ by which the nickel ion intercalation within the crystalline lattice structure of the α-ZrP (Pümpel et al., 2003). Furthermore, the ion exchange, which always results in H^+ release (Eq. (4)) illustrates the binding of Ni (*II*) onto the *α*-ZrP-n which led to the enhancement of Ni (*II*) removal when compared to pristine cellulose membrane (Fig. 7.) (Pan et al., 2007a). The Zeta potential results (Fig. 6) showed that both the pristine cellulose membrane and the *α*-ZrP-n are negatively charged at pH = 7. Initially, the attraction between the Ni (*II*) and the cellulose membrane can be observed (Fig. 7). Following that, with an *α*-ZrP-n

coating, the negative surface charge of the membrane increases leading to enhanced removal of the Ni (*II*) due to electrostatic attraction forces. The Ni (*II*) and $Zr(HPO_4)_2 \cdot H_2O$ ion exchange can possibly happen according to the following two equations (Eqs. (5), (6)):

$$Zr(HPO_4)_2 \cdot H_2O + 0.5Ni^{2+} + 5H_2O \rightleftharpoons ZrNi_{0.5}H(PO_4)_2 \cdot 5H_2O + H^+ + H_2O \quad (5)$$

$$ZrNi_{0.5}H(PO_4)_2 \cdot 5H_2O + 0.5Ni^{2+} \rightleftharpoons ZrNi(PO_4)_2 \cdot 3H_2O + H^+ + 2H_2O \quad (6)$$

Similarly, the removal of Zn (*II*) has improved in the *α*-ZrP-n coated membranes when compared to the pristine cellulose (Fig. 7). This enhancement can be attributed to the possible ion exchange illustrated in Eqs. (7), (8). The zinc speciation at pH = 7 shows that the dominant species of Zn is in the form of Zn (*II*) (Krężel and Maret, 2016):

$$Zr(HPO_4)_2 \cdot H_2O + 0.5Zn^{2+} + 5H_2O \rightleftharpoons ZrZn_{0.5}H(PO_4)_2 \cdot 5H_2O + H^+ + H_2O \quad (7)$$

$$ZrZn_{0.5}H(PO_4)_2 \cdot 5H_2O + 0.5Zn^{2+} \rightleftharpoons ZrZn(PO_4)_2 \cdot 3H_2O + H^+ + 2H_2O \quad (8)$$

Furthermore, both Pb (*II*) and Cu (*II*) followed the same improvement trend in removal percentage as Zn (*II*) and Ni (*II*) respectively. The stoichiometric ion exchange equation of the metal ions onto the α-ZrP-n explained earlier (Eq. (4)) can be used to represent the possible ion exchange for both Pb (*II*) and Cu (*II*) with $Zr(HPO_4)_2 \cdot H_2O$. Furthermore, as can be observed from the results in Fig. 7, Pb (*II*) has the highest removal followed by Cu (*II*), Zn (*II*), and Ni (*II*). In an aqueous solution with competing cations (i.e. Cu (*II*), Ni(*II*), Pb (*II*), and Zn (*II*)), α-ZrP-n has a higher affinity (favorable sorption) towards Pb (*II*) (Hua et al., 2013; Pan et al., 2007a). This could be related to the Gibbs free energies (or hydration energies of ions) which play a significant role in the ion exchange preference. The adsorption is mostly favored towards cations with lower hydration energies (Hua et al., 2013). Among the four heavy metal ions used in this study, Pb (*II*) has the lowest hydration energy (ΔH of around −1481 kJ/mol) (Cotton and Wilkinson, 1980) and hence, adsorption was favored towards it. This explains the increased removal of Pb (*II*) at similar pH when compared to Ni (*II*) that has hydration energy of −2105 kJ/mol (Cotton and Wilkinson, 1980). In other words, the increased removal could be related to the metal's first hydrolysis constant (Eq. (9)). Adsorbents (*α*-ZrP-n in this case) have in general higher affinity towards metals with lower hydrolysis constant (Hua et al., 2013; Pagnanelli et al., 2003; Pan et al., 2007a). The hydrolysis constant of all the heavy metals used in this study is summarized in Table S2.

$$HO{-}H + M^{2+} \rightarrow M(OH)^+ + H^+ \quad (9)$$

It is evident from Table S2 that the metal hydrolysis constant is in the order of Pb (*II*) < Cu (*II*) < Zn (*II*) < Ni (*II*). This implies that the uppermost adsorbent (α-ZrP-n) affinity would be in favor of Pb (II) followed by Cu (*II*), Zn (*II*), and Ni (*II*). This explains the highest removal of Pb (*II*) (as shown in Fig. 7), followed by the rest of the heavy metals in the following order: Pb (*II*) > Cu (*II*) > Zn (*II*) > Ni (*II*). For example, when ZrP-C4 was used, the removal of Pb (*II*), Cu (*II*), Zn (*II*), and Ni (*II*) was 61.3 ± 2.1, 58.1 ± 1.6, 28.7 ± 2.1, and 15.5 ± 1.2%, respectively. The rest of the *α*-ZrP-n coated membranes followed a similar trend. Overall, the impregnation of the nano-sized *α*-ZrP-n provided a higher surface area and created several ions binding sites on the membrane's surface which significantly enhanced the capture capacity of the heavy metals (Hua et al., 2013).

After filtration tests, all membranes were characterized using EDS to demonstrate the adsorption of all heavy metals onto the membrane's surface and the results are summarized in Fig. 8. All membranes showed heavy metal deposition on their surface which confirms the adsorption of these metal ions. These results are in accordance with the results illustrated in Fig. 7. The unique characteristic peak of Ni (*II*) can be seen at L*α* = 0.851 keV, Cu (*II*) at L*α* = 0.930 keV, Zn (*II*) at L*α* = 1.012 keV, and Pb (*II*) at L*α* = 2.342 keV.

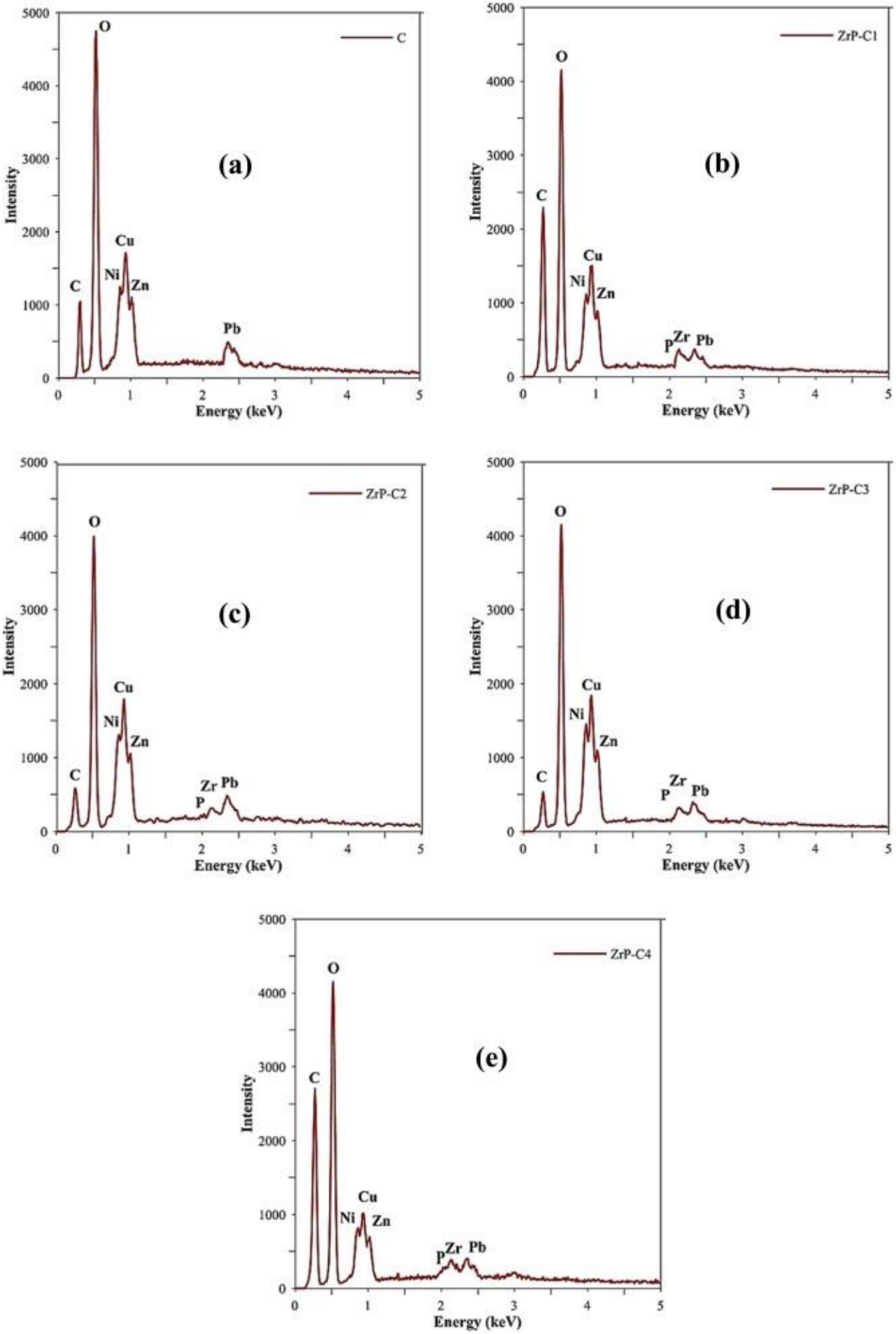
(a)
C
O
Cu
Ni
Zn
Pb
Intensity
Energy (keV)
(b)
ZrP-C1
O
C
Cu
Ni
Zn
P
Zr
Pb
Intensity
Energy (keV)
(c)
ZrP-C2
O
Cu
Ni
Zn
C
Zr
Pb
P
Intensity
Energy (keV)
(d)
ZrP-C3
O
Cu
Ni
Zn
C
P
Zr
Pb
Intensity
Energy (keV)
(e)
ZrP-C4
O
C
Cu
Ni
Zn
P
Zr
Pb
Intensity
Energy (keV)

Fig. 8. EDS analysis results of the pristine cellulose and *α*-ZrP-n incorporated membranes after filtration tests: (a) C, (b) ZrP-C1, (c) ZrP-C2, (d) ZrP-C3, and (e) ZrP-C4.

Although EDS is a useful technique in identifying the chemical elements of the sample, it cannot be used accurately to quantify trace elements with concentrations >500 mg/L (Goldstein et al., 2018; Liao, 2006). Therefore, the elemental intensity peaks in Fig. 8 cannot be used to quantify the concentration of heavy metals which were removed.

3.3. Impact of wastewater pH on the removal of heavy metals

Acidity plays a critical role in the removal of ions in aqueous solutions since it affects ionic chemistry such as hydrolysis, coordination, redox reactions, etc. In addition, it influences the ionic state of the adsorbents. Therefore, the impact of pH on heavy metal removal was investigated and the results are shown in Fig. 9. It was observed that the increase in solution pH led to a remarkable increase in the metal ion uptake. For example, Zn (*II*) removal efficiency in ZrP-C1 membrane increased from 28.2 ± 1.7% at pH = 7 (Fig. 9(a)) to 98.2 ± 0.7% at pH = 12. On the other hand, at a very low pH (i.e. pH = 2), the removal efficiency decreased significantly (i.e. from 28.2 ± 1.7% at pH = 7 to 8.2 ± 1.1% at pH = 2). Similar trends were observed for the rest of the metal ions in the pristine cellulose and other *α*-ZrP-n surface coated membranes (Fig. 9(b), (c), and (d)) where the heavy metal attained complete removal at pH between 10 and 12. Additionally, at a very low pH, the metal ion adsorption is restricted through the high competition of H^+ as illustrated by Eq. (7) where the majority of the OH^- groups on the cellulose membrane's surface get protonated. The active binding sites (in the protonated form) on the adsorbent (*α*-ZrP-n) get abated which is in accordance with the Le Châtelier principle of ion exchange (Eq. (4)) (Pagnanelli et al., 2003; Pan et al., 2007b). These two effects are in agreement with the zeta potential results obtained earlier (Fig. 6) for the pristine cellulose membrane surface and *α*-ZrP-n. The surface charge negativity fades considerably with the decrease of pH through which it becomes positive at pH = 5 and 3.1 for the pristine cellulose membrane and *α*-ZrP-n, respectively. This could hinder the interaction between the heavy metals and the active sites on the membrane's surface which explains the low uptake of metal ions at a very low pH value.

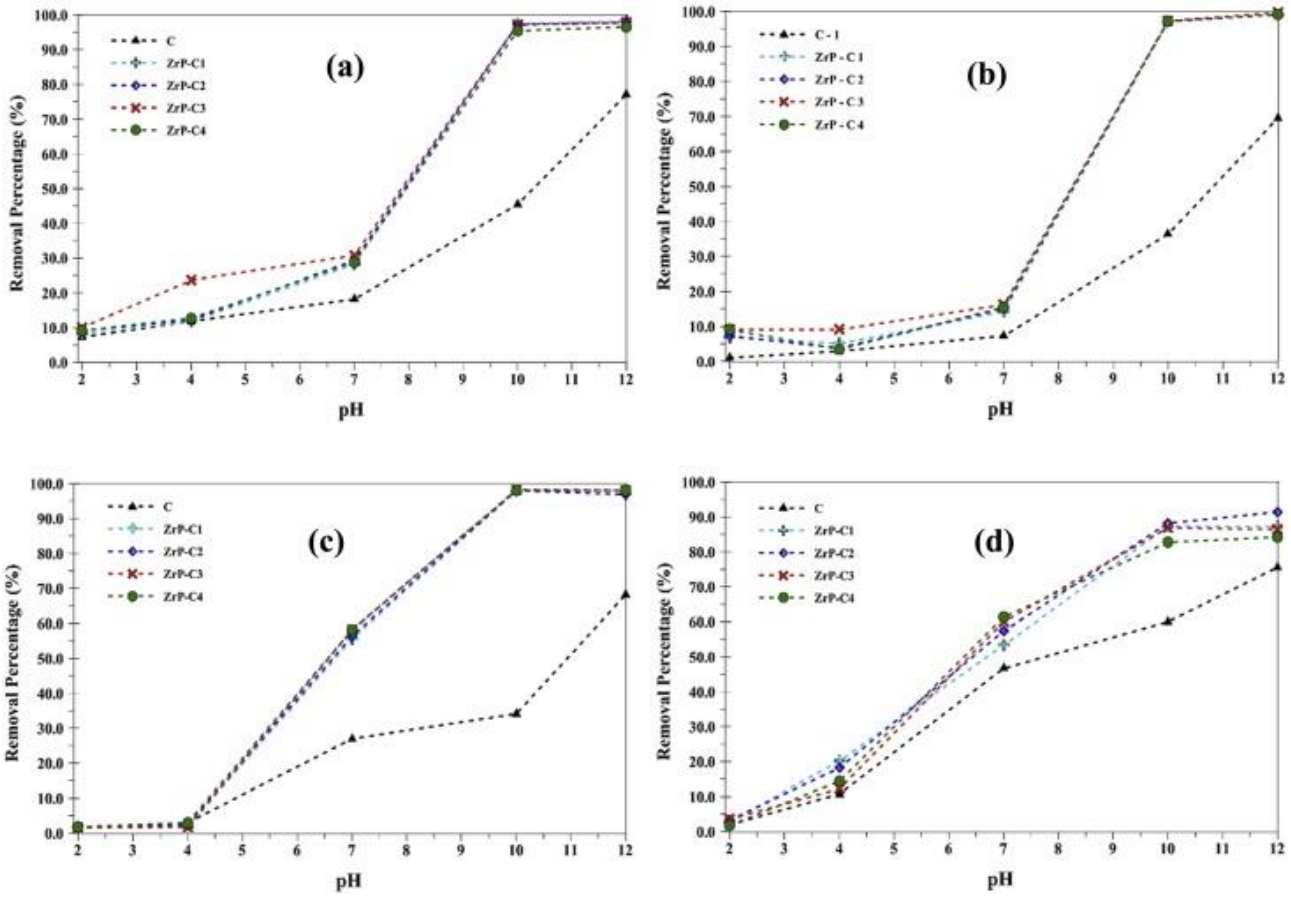

Fig. 9. pH impact on the overall removal of (a) Zn (*II*), (b) Ni (*II*), (c) Cu (*II*), and (d) Pb (*II*).

The chemistry of the ions in the solution is greatly affected by the increase of pH in the solution. For example, increasing the pH grants the metal ions the ability to form insoluble complex hydroxides as a result of interaction with the abundant OH^- groups found at high pH values (Ozaki et al., 2002). In an aqueous solution with pH = 7, the predominant zinc species is in the form of Zn (*II*) (Krężel and Maret, 2016). However, with further increase in pH, different ions complexes such as $ZnOH^+$, $Zn(OH)_{2(aq)}$, $Zn(OH)_{2(s)}$, $Zn(OH)_3^-$, and $Zn(OH)_4^{-2}$ are formed. Similarly, at neutral conditions, nickel dominant species is in the form of Ni (*II*). The increase of pH results in the forming of $NiOH^+$, $Ni(OH)_{2(aq)}$, $Ni(OH)_{2(s)}$, $Ni(OH)_3^-$, and $Ni(OH)_4^{-2}$ (Ji and Cooper, 1996). When pH is between 10 and 12, the dominate Ni hydroxide is in the form of $Ni(OH)_{2(s)}$ (Ji and Cooper, 1996). Both Pb (*II*) and Cu (*II*) tend to form metal hydroxides when pH of the solution was increased, an occurrence observed in several other studies (Jiang et al., 2010; Kongsuwan et al., 2009; Sen Gupta and Bhattacharyya, 2008). Metal hydroxides have larger molecules that are incapable of passing through the membrane's pores and precipitate on the surface of the membrane. Therefore, the removal of all heavy metals at pH = 12 using pristine cellulose membrane was in the range of 65–75%. On the other

hand, the removal increased to 99% using the *α*-ZrP-n coated membranes with the exception of Pb (*II*). This is due to its high diffusion coefficientcompared to the rest of heavy metals facilitates the passage through the membrane (Vanysek, 2005). Furthermore, the superior removal in the *α*-ZrP-n coated membranes compared to the pristine cellulose at high pH could possibly be attributed to the enhanced adsorption and binding strength of the actives sites on the adsorbent (*α*-ZrP) surface and the co-precipitate and/or the complex hydroxides. This is related to the substantial increase of the OH^- density on the *α*-ZrP-n surface that was confirmed through the zeta potential results obtained earlier (Fig. 6). Zeta potential results showed a significant increase in the *α*-ZrP-n surface negativity with the increase of the solution pH. Complex hydroxides lead to the formation of a cake layer on top of the membrane surface via hydroxides precipitation. As a result, the membrane undergoes significant flux reduction due to membrane fouling as has been illustrated in Fig. 5. As could be observed from both figures (Fig. 5, Fig. 9), the highest heavy metal removal at pH = 12 led to substantial flux decrease. The C membrane which reported a lower removal at pH = 12, had lesser flux decline compared to the rest of the membranes (ZrP-C1, ZrP-C2, ZrP-C3, and ZrP-C4). This illustration is valid for the effect of pH on the removal and flux performance. Hence the highest removal is always accompanied by the highest flux decline.

To further investigate the flux decline, the surface and cross-sectional morphologies of the membranes after filtration were evaluated using SEM imaging (Fig. 10). It was observed that heavy metals were deposited on the cellulose membrane fibers that subsequently formed a cake layer. This layer is more noticeable in the *α*-ZrP-n surface coated membranes due to their high affinity to the metal ions and hydroxides. The cross-sectional images showed that most of this deposition happened on the surface of the membranes (Fig. 10). The removal efficiency of the present cellulose/*α*-ZrP-n enhanced membranes has been compared with other cellulose-based membranes reported for heavy metal removal (Table 2). When compared to other cellulose-based membranes, the novel cellulose/*α*-ZrP-n surface-coated membrane showed superiority with respect to the removal of heavy metals from metal mixture wastewater solution.

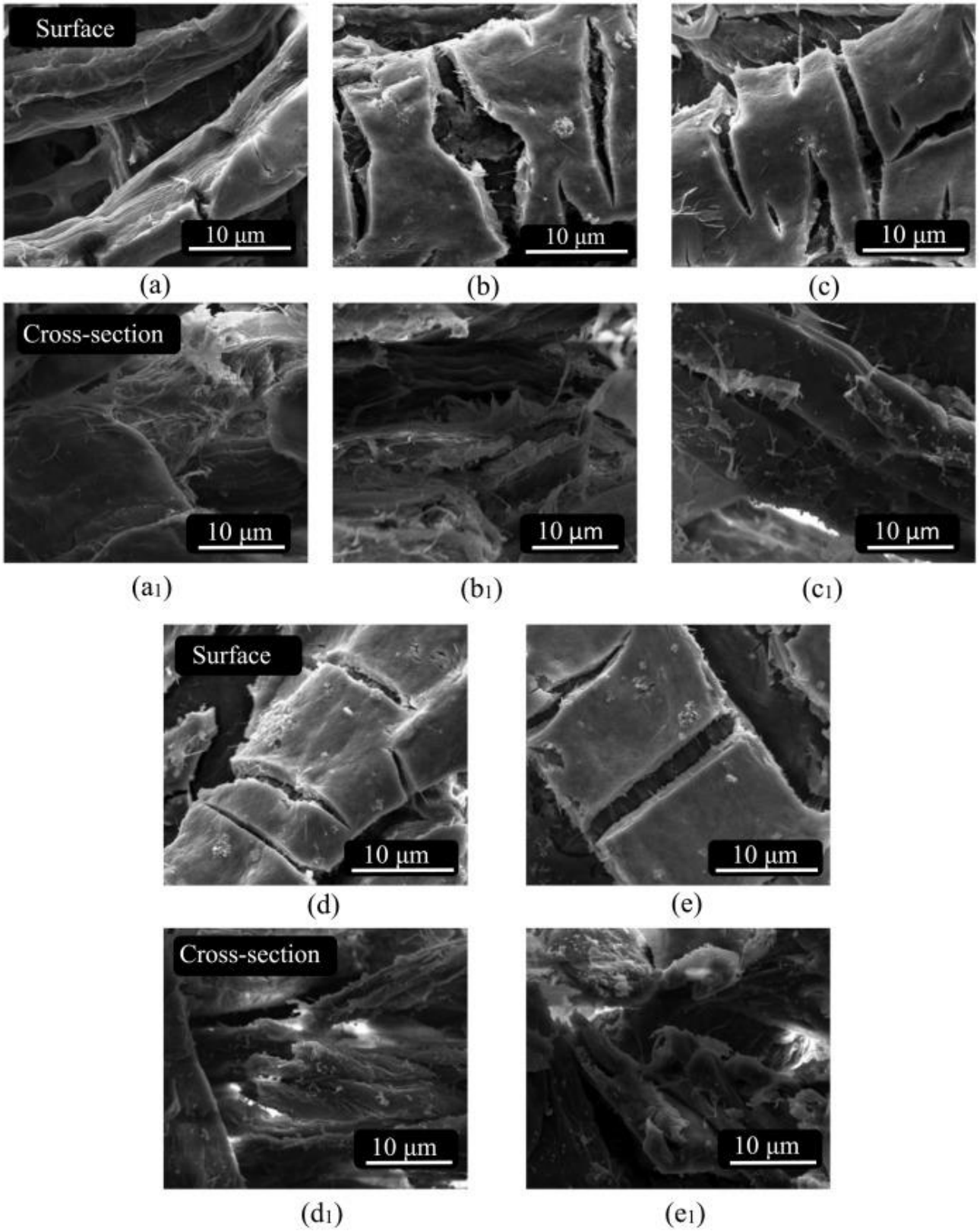

Fig. 10. Surface and cross-sectional morphology of the membranes after filtration: (a, a1) pristine cellulose membrane, (b, b_1) ZrP-C1, (c, c_1) ZrP-C2, (d, d_1) ZrP-C3, and (e, e_1) ZrP-C4.

Table 2. Comparison of different cellulose-based membranes with cellulose/α-ZrP-n surface-coated membranes fabricated in this study.

Membrane material	Modified with	pH	Heavy metal(s)	Removal	Ref.
Cellulose	PVA	7	Cu (*II*)	~45%	(Çifci and Kaya, 2010)
Cellulose acetate	Zeolites	6	Ni (*II*)	~80%	(Ji et al., 2012)
Cellulose	Methyl benzalaniline	10	Pb (*II*) and Cu (*II*)	~70% and ~60%	(Saravanan and Ravikumar, 2015)
Cellulose	EDTA	9	Pb (*II*)	~90%	D'Halluin et al. (2017)
Cellulose	α-ZrP-n	10	Pb (*II*), Ni (*II*), and Cu (*II*).	88%, 97%, and 98%	This work

4. Conclusions

This research study focused on the synthesis and characterization of novel cellulose membranes via surface coating with α-ZrP-n for the removal of heavy metals from wastewater. It was concluded that the surface coated membranes were super hydrophilic reporting a contact angle of 0^{o}. Furthermore, SEM images revealed dense rode-shaped porous fibers network. The porosity of the C, ZrP-C1, ZrP-C2, ZrP-C3, and ZrP-C4 were 65, 60, 54, 48, and 48%, respectively. ZrP-C1 reported the highest pure water flux of $61.00 \pm 0.20 \times 10^{3}$ LMH. It was also observed that ZrP-C4 possessed the maximum tensile strength of 4 MPa as well as the highest decomposition temperature of 285 °C. Furthermore, heavy metal removal for all membranes used in this study (at pH = 7) was in the following order: Pb (*II*) > Cu (*II*) > Zn (*II*) > Ni (*II*). This was attributed to the Gibbs free energies (or hydration energies of ions) which played a significant role in the ion exchange preference. The highest removal efficiency at neutral conditions was observed for ZrP-C4 with 61.3 ± 2.1, 58.1 ± 1.6, 28.7 ± 2.1, and 15.5 ± 1.2% for Pb (*II*), Cu (*II*), Zn (*II*), and Ni (*II*), respectively. This removal improvement (compared to the pristine cellulose membrane) was attributed to the increased number of binding sites for metal ions on the surface of the membrane as a result of the α-ZrP-n surface coating. In addition, increasing the pH of the wastewater has led to an increase in removal efficiency. For example, ZrP-C2 reported 97.0 ± 0.6, 98.0 ± 0.5, 99.5 ± 0.2, and 91.5 ± 2.0% for Cu (*II*), Zn (*II*), Ni (*II*), and Pb (*II*), respectively. The high removal percentage was due to the enhanced adsorption and binding strength of the active sites and the co-precipitate and/or the complex hydroxides. The main mechanisms behind metal removal were the electrostatic attraction between the heavy metal ions and the high-negatively charged membrane's surface as well as an ion exchange of the metal ions with the α-ZrP-n.

Overall, it was concluded that cellulose-zirconium phosphate based membranes could be used to selectively eliminate heavy metal ions from wastewater. Incorporation of nano-sized α-ZrP-n on the MFcellulose membranes has the potential of achieving high heavy metal removal and reducing the specific energy requirements due to the very low-pressure requirements and the relatively high water flux.

Declaration of Competing Interest

None of the authors has conflicting interests.

Acknowledgment

Authors appreciate the support of Khalifa University of Science and Technology in Abu Dhabi (UAE). Special thanks to Dr. Cyril Aubry for his help and assistance in conducting the microscopy analysis.

Appendix A. Supplementary data

Supplementary data to this article can be found online at https://doi.org/10.1016/j.scitotenv.2019.07.009.

References

Abutartour, A., Jia, Y., Majdoub, L. El, Xu, Q., 2014. A new hierarchical porous zirconium phosphate membrane and its adsorption properties. Microporous Mesoporous Mater. 196, 1–7. https://doi.org/10.1016/j.micromeso.2014.04.054.

Ahmed, M.A.L., Hasan, S.W., 2017. Fe and Zn removal from steel making industrial wastewater by electrically enhanced membrane bioreactor. Desalin. Water Treat. 93, 9–21. https://doi.org/10.5004/dwt.2017.21305.

Ali, N., Zaman, H., Bilal,M., Shah, A. ul H.A., Nazir,M.S., Iqbal, H.M.N., 2019. Environmental perspectives of interfacially active and magnetically recoverable composite materials a review. Sci. Total Environ. 670, 523–538. https://doi.org/10.1016/j.scitotenv.2019.03.209.

Apiratikul, R., Pavasant, P., 2008. Sorption of Cu2+, Cd2+, and Pb2+ using modified zeolite from coal fly ash. Chem. Eng. J. 144, 245–258. https://doi.org/10.1016/j.cej.2008.01.038.

Arepalli, S., Nikolaev, P., Gorelik, O., Hadjiev, V.G., Holmes, W., Files, B., Yowell, L., 2004.Protocol for the characterization of single-wall carbon nanotubematerial quality. Carbon N. Y. 42, 1783–1791. https://doi.org/10.1016/j.carbon.2004.03.038.

Barud, H.S., Assunção, R.M.N., Martines, M.A.U., Dexpert-Ghys, J., Marques, R.F.C., Messaddeq, Y., Ribeiro, S.J.L., 2008. Bacterial cellulose-silica organic-inorganic hybrids. J. Sol-Gel Sci. Technol. 46, 363–367. https://doi.org/10.1007/s10971-007-1669-9.

Barud, H.S., Souza, J.L., Santos, D.B., Crespi, M.S., Ribeiro, C.A., Messaddeq, Y., Ribeiro, S.J.L., 2011. Bacterial cellulose/poly(3-hydroxybutyrate) composite membranes. Carbohydr. Polym. 83, 1279–1284. https://doi.org/10.1016/j.carbpol.2010.09.049.

Basile, A., Cassano, A., Rastogi, N.K., 2015. Advances inMembrane Technologies for Water Treatment: Materials, Processes and Applications. Elsevier, Amsterdam https://doi.org/10.1016/C2013-0-16469-0.

Benateau, S., Gaudard, A., Stamm, C., Altermatt, F., 2019. Climate Change and Freshwater Ecosystems: Impacts on Water Quality and Ecological Status. Federal Office for the Environment (FOEN) & Eawag, Bern https://doi.org/10.5167/uzh-169641.

Bhattacharyya, D., Hestekin, J.A., Brushaber, P., Cullen, L., Bachas, L.G., Sikdar, S.K., 1998. Novel poly-glutamic acid functionalized microfiltration membranes for sorption of heavy metals at high capacity. J. Memb. Sci. 141, 121–135. https://doi.org/10.1016/S0376-7388(97)00301-3.

Bolisetty, S., Peydayesh, M., Mezzenga, R., 2019. Sustainable technologies for water purification from heavy metals: review and analysis. Chem. Soc. Rev. 48, 463–487. https://doi.org/10.1039/c8cs00493e.

Cai, X., Dai, G.J., Tan, S.Z., Ouyang, Y., Ouyang, Y.S., Shi, Q.S., 2012. Synergistic antibacterial zinc ions and cerium ions loaded α-zirconium phosphate. Mater. Lett. 67, 199–201. https://doi.org/10.1016/j.matlet.2011.09.041.

Chalkova, E., Fedkin, M.V., Komarneni, S., Lvov, S.N., 2007. Nafion/zirconium phosphate composite membranes for PEMFC operating at up to 120°C and down to 13% RH. J. Electrochem. Soc. 154, 288–295. https://doi.org/10.1149/1.2405731.

Çifci, C., Kaya, A., 2010. Preparation of poly(vinyl alcohol)/cellulose composite membranes for metal removal from aqueous solutions. Desalination 253, 175–179. https://doi.org/10.1016/j.desal.2009.11.010.

Cotton, F.A., Wilkinson, G., 1980. Advanced Inorganic Chemistry, Advanced Inorganic Chemistry. Wiley, New York.

Danilenko, I., Konstantinova, T., Pilipenko, N., Volkova, G., Glasunova, V., 2012. Estimation of agglomeration degree and nanoparticles shape of zirconia nanopowders. Part. Part. Syst. Charact. 28, 1–6. https://doi.org/10.1002/ppsc.200800041.

Daniş, Ü., Keskinler, B., 2009. Chromate removal from wastewater using micellar enhanced crossflow filtration: effect of transmembrane pressure and crossflow velocity. Desalination 249, 1356. https://doi.org/10.1016/j.desal.2009.06.023.

D'Halluin,M., Rull-Barrull, J., Bretel, G., Labrugère, C., Le Grognec, E., Felpin, F.X., 2017. Chemicallymodified cellulose filter paper for heavymetal remediation inwater. ACS Sustain. Chem. Eng. 5, 1965–1973. https://doi.org/10.1021/acssuschemeng.6b02768.

Feng, Y., He,W., Zhang, X., Jia, X., Zhao,H., 2007. The preparation of nanoparticle zirconium phosphate. Mater. Lett. 61, 3258–3261. https://doi.org/10.1016/j.matlet.2006.11.132.

Fu, F., Wang, Q., 2011. Removal of heavy metal ions from wastewaters: a review. J. Environ. Manag. 92, 407–418. https://doi.org/10.1016/j.jenvman.2010.11.011.

Garside, P., Wyeth, P., 2003. Identification of cellulosic Fibres by FTIR spectroscopy - thread and single fibre analysis by attenuated total reflectance. Stud. Conserv. 48,269–275. https://doi.org/10.1179/sic.2003.48.4.269.

Giwa, A., Jung, S.M., Ahmed, M., Fang, W., Kong, J., Hasan, S.W., 2018. Selectivity of nanoporous MnO2 and TiO2 membranes for residual contaminants in treated wastewater. Chem. Eng. Technol. 41, 413–420. https://doi.org/10.1002/ceat.201700376.

Goldstein, J.I., Newbury, D.E., Michael, J.R., Ritchie, N.W.M., Scott, J.H.J., Joy, D.C., 2018. Scanning Electron Microscopy and X-Ray Microanalysis. Fourth. ed. Springer, New York https://doi.org/10.1007/978-1-4939-6676-9.

Han, L., Chen, Q., Chen, H., Yu, S., Xiao, L., Ye, Z., 2018. Synthesis and performance of functionalized alpha-zirconium phosphate modified with octadecyl isocyanate. J. Nanomater. 2018, 9. https://doi.org/10.1155/2018/5873871.

He, J., Kunitake, T., Nakao, A., 2003. Facile in situ synthesis of noble metal nanoparticles in porous cellulose fibers. Chem. Mater. (23), 4401–4406 https://doi.org/10.1021/cm034720r.

He, J., Matsuura, T., Chen, J.P., 2014. A novel Zr-based nanoparticle-embedded PSF blend hollow fiber membrane for treatment of arsenate contaminated water: material development, adsorption and filtration studies, and characterization. J. Memb. Sci. 452, 433–445. https://doi.org/10.1016/j.memsci.2013.10.041.

Hua, M., Jiang, Y., Wu, B., Pan, B., Zhao, X., Zhang, Q., 2013. Fabrication of a newhydrous Zr (IV) oxide-based nanocomposite for enhanced Pb(II) and Cd(II) removal from waters. ACS Appl. Mater. Interfaces 5 (22), 12135–12142. https://doi.org/10.1021/am404031q.

Huang, T.-C., Lai, G.-H., Li, C.-E., Tsai, M.-H., Wan, P.-Y., Chung, Y.-H., Lin, M.-H., 2017. Advanced anti-corrosion coatings prepared from α-zirconium phosphate/polyurethane nanocomposites. RSC Adv. 7, 9908–9913. https://doi.org/10.1039/C6RA27588E.

Huisman, I.H., 2000. Membrane separations | microfiltration. In: Wilson, I.D. (Ed.), Encyclopedia of Separation Science. Academic Press, Oxford, pp. 1764–1777 https://doi.org/10.1016/B0-12-226770-2/05251-0.

Ibrahim, Y., Arafat, H.A., Mezher, T., AlMarzooqi, F., 2018. An integrated framework for sustainability assessment of seawater desalination. Desalination 447, 1–17. https://doi.org/10.1016/J.DESAL.2018.08.019.

Ji, J., Cooper,W.C., 1996. Nickel speciation in aqueous chloride solutions. Electrochim. Acta 41, 1549–1560. https://doi.org/10.1016/0013-4686(95)00407-6.

Ji, F., Li, C., Tang, B., Xu, J., Lu, G., Liu, P., 2012. Preparation of cellulose acetate/zeolite composite fiber and its adsorption behavior for heavy metal ions in aqueous solution. Chem. Eng. J. 209, 325–333. https://doi.org/10.1016/j.cej.2012.08.014.

Jiang,M., Jin, X., Lu, X.-Q., Chen, Z., 2010. Adsorption of Pb(II), Cd(II), Ni(II) and Cu(II) onto natural kaolinite clay. Desalination 252, 33–39. https://doi.org/10.1016/j.desal.2009.11.005.

Kabbashi, N.A., Atieh,M.A., Al-Mamun, A.,Mirghami,M.E.S., Alam, M.D.Z., Yahya, N., 2009. Kinetic adsorption of application of carbon nanotubes for Pb(II) removal

from aqueous solution. J. Environ. Sci. 21, 539–544. https://doi.org/10.1016/S1001-0742(08)62305-0.
Kamel, S., Hassan, E.M., El-Sakhawy, M., 2006. Preparation and application of acrylonitrile-grafted cyanoethyl cellulose for the removal of copper (II) ions. J. Appl. Polym. Sci. 100, 329–334. https://doi.org/10.1002/app.23317.
Karlsson, M., Andersson, C., Hjortkjaer, J., 2001. Hydroformylation of propene and 1-hexene catalysed by a α-zirconium phosphate supported rhodium-phosphine complex. J. Mol. Catal. A Chem. 166, 337–343. https://doi.org/10.1016/S1381-1169(00)00480-5.
Köhler, S.J., Cubillas, P., Rodríguez-Blanco, J.D., Bauer, C., Prieto, M., 2007. Removal of cadmium from wastewaters by aragonite shells and the influence of other divalent cations. Environ. Sci. Technol. 41, 112–118. https://doi.org/10.1021/es060756j.
Kongsuwan, A., Patnukao, P., Pavasant, P., 2009. Binary component sorption of Cu (II) and Pb (II) with activated carbon from Eucalyptus camaldulensis Dehn bark. J. Ind. Eng. Chem. 15, 465–470. https://doi.org/10.1016/j.jiec.2009.02.002.
Krężel, A., Maret,W., 2016. The biological inorganic chemistry of zinc ions. Arch. Biochem. Biophys. 611, 3–19. https://doi.org/10.1016/j.abb.2016.04.010.
Li, Y., Liu, F., Xia, B., Du, Q., Zhang, P.,Wang, D.,Wang, Z., Xia, Y., 2010. Removal of copper from aqueous solution by carbon nanotube/calcium alginate composites. J. Hazard.Mater. 177, 876–880. https://doi.org/10.1016/j.jhazmat.2009.12.114.
Liao, Y., 2006. Practical Electron Microscopy and Database. https://www.globalsino.com/EM/, Accessed date: 20 March 2019.
van Loosdrecht, M.C.M., Brdjanovic, D., 2014. Anticipating the next century of wastewater treatment. Science 344, 1452–1453. https://doi.org/10.1126/science.1255183.
Madaeni, S.S., Heidary, F., 2012. Effect of surface modification of microfiltration membrane on capture of toxic heavy metal ions. Environ. Technol. 33, 393–399. https://doi.org/10.1080/09593330.2011.576703.
Maneerung, T., Tokura, S., Rujiravanit, R., 2008. Impregnation of silver nanoparticles into bacterial cellulose for antimicrobial wound dressing. Carbohydr. Polym. 72, 43–51. https://doi.org/10.1016/j.carbpol.2007.07.025.
Mansour, S., Giwa, A., Hasan, S.W., 2018. Novel graphene nanoplatelets-coated polyethylene membrane for the treatment of reject brine by pilot-scale direct contact membrane distillation: an optimization study. Desalination 441, 9–20. https://doi.org/10.1016/j.desal.2018.04.026.
Mohan, T., Kargl, R., Doliška, A., Vesel, A., Köstler, S., Ribitsch, V., Stana-Kleinschek, K., 2011. Wettability and surface composition of partly and fully regenerated cellulose thin films from trimethylsilyl cellulose. J. Colloid Interface Sci. 358, 604. https://doi.org/10.1016/j.jcis.2011.03.022.
Mohod, C.V., Dhote, J., 2013. Review of heavy metals in drinking water and their effect on human health. Int. J. Innov. Res. Sci. Eng. Technol. (ISSN: 2278-0181) 2, 2992–2996.
Mulinari, D.R., Voorwald, H.J.C., Cioffi, M.O.H., da Silva, M.L.C.P., da Cruz, T.G., Saron, C., 2009. Sugarcane bagasse cellulose/HDPE composites obtained by extrusion. ComposSci. Technol. 69, 214–219. https://doi.org/10.1016/j.compscitech.2008.10.006.

Nabeel, F., Rasheed, T., Bilal,M., Iqbal, H.M.N., 2019. upramolecularmembranes: a robust platform to develop separation strategies towards water-based applications. Sep. Purif. Technol. 215, 411–453. https://doi.org/10.1016/j.seppur.2019.01.035.

Oh, S.Y., Dong, I.Y., Shin, Y., Hwan, C.K., Hak, Y.K., Yong, S.C.,Won, H.P., Ji, H.Y., 2005. Crystalline structure analysis of cellulose treatedwith sodiumhydroxide and carbon dioxide by means of X-ray diffraction and FTIR spectroscopy. Carbohydr. Res. 340, 2376–2391. https://doi.org/10.1016/j.carres.2005.08.007.

Ozaki, H., Sharma, K., Saktaywin, W., 2002. Performance of an ultra-low-pressure reverse osmosismembrane (ULPROM) for separating heavy metal: effects of interference parameters. Desalination 144, 287–294. https://doi.org/10.1016/S0011-9164(02)00329-6.

Pagnanelli, F., Esposito, A., Toro, L., Vegliò, F., 2003. Metal speciation and pH effect on Pb, Cu, Zn and Cd biosorption onto Sphaerotilus natans: Langmuir-type empirical model. Water Res. 37, 627–633. https://doi.org/10.1016/S0043-1354(02)00358-5.

Pan, Zhang, Q.R., Zhang, W.M., Pan, B.J., Du, W., Lv, L., Zhang, Q.J., Xu, Z.W., Zhang, Q.X., 2007a. Highly effective removal of heavy metals by polymer-based zirconium phosphate: a case study of lead ion. J. Colloid Interface Sci. 310, 99–105. https://doi.org/10.1016/j.jcis.2007.01.064.

Pan, Zhang, Qingrui, Du, W., Zhang, W., Pan, B., Zhang, Qingjian, Xu, Z., Zhang, Quanxing, 2007b. Selective heavy metals removal from waters by amorphous zirconium phosphate: behavior and mechanism. Water Res. 41, 3103–3111. https://doi.org/10.1016/j.watres.2007.03.004.

Patel, H., Chudasama, U., 2007. A comparative study of proton transport properties of metal (IV) phosphates. J. Chem. Sci. 119, 35–40. https://doi.org/10.1007/s12039-007-0006-8.

Pourbeyram, S., 2016. Effective removal of heavy metals from aqueous solutions by graphene oxide–zirconium phosphate (GO–Zr-P) nanocomposite. Ind. Eng. Chem. Res. 55, 5608–5617. https://doi.org/10.1021/acs.iecr.6b00728.

Pümpel, T., Macaskie, L.E., Finlay, J.A., Diels, L., Tsezos, M., 2003. Nickel removal from nickel plating waste water using a biologically active moving-bed sand filter. BioMetals 16, 567–581. https://doi.org/10.1023/A:1023476625820.

Raghavendra, G.M., Jayaramudu, T., Varaprasad, K., Sadiku, R., Ray, S.S., Mohana Raju, K., 2013. Cellulose-polymer-Ag nanocomposite fibers for antibacterial fabrics/skin scaffolds. Carbohydr. Polym. 93, 533–560. https://doi.org/10.1016/j.carbpol.2012.12.035.

Rasheed, T., Bilal, M., Nabeel, F., Iqbal, H.M.N., Li, C., Zhou, Y., 2018. Fluorescent sensor based models for the detection of environmentally-related toxic heavy metals. Sci. Total Environ. 615, 476–485. https://doi.org/10.1016/j.scitotenv.2017.09.126.

Ristić, T., Mohan, T., Kargl, R., Hribernik, S., Doliška, A., Stana-Kleinschek, K., Fras, L., 2014. A study on the interaction of cationized chitosan with cellulose surfaces. Cellulose 21, 2315–2325. https://doi.org/10.1007/s10570-014-0267-6.

Ritchie, S.M.C., Bachas, L.G., Olin, T., Sikdar, S.K., Bhattacharyya, D., 1999. Surface modification of silica- and cellulose-based microfiltration membranes with functional polyamino acids for heavy metal sorption. Langmuir 15, 6346–6357. https://doi.org/10.1021/la9814438.

Saljoughi, E., Sadrzadeh, M.,Mohammadi, T., 2009. Effect of preparation variables onmorphology and purewater permeation flux through asymmetric cellulose acetatemembranes. J. Memb. Sci. 326, 627–634. https://doi.org/10.1016/j.memsci.2008.10.044.

Saravanan, R., Ravikumar, L., 2015. The Use of New Chemically Modified Cellulose for Heavy Metal Ion Adsorption and Antimicrobial Activities. J. Water Resour. Prot. 7, 530–545. https://doi.org/10.4236/jwarp.2015.76042.

Schwartz, F.W., Ibaraki, M., 2011. Groundwater: a resource in decline. Elements 7, 175–179. https://doi.org/10.2113/gselements.7.3.175.

Sen Gupta, S., Bhattacharyya, K.G., 2008. Immobilization of Pb(II), Cd(II) and Ni(II) ions on kaolinite andmontmorillonite surfaces from aqueousmedium. J. Environ.Manag. 87, 46–58. https://doi.org/10.1016/j.jenvman.2007.01.048.

Steduto, P., Hoogeveen, J., Winpenny, J., Burke, J., 2017. Coping with Water Scarcity: An Action Framework for Agriculture and Food Security. Food and Agriculture Organization of the United Nations, Rome.

Su, Y., Cui, H., Li, Q., Gao, S., Shang, J.K., 2013. Strong adsorption of phosphate by amorphous zirconium oxide nanoparticles. Water Res. 47, 5018–5026. https://doi.org/10.1016/j.watres.2013.05.044.

Sun, L., Boo, W.J., Sue, H.J., Clearfield, A., 2007. Preparation of alpha-zirconium phosphate nanoplatelets with wide variations in aspect ratios. New J. Chem. 31, 39. https://doi.org/10.1039/b604054c.

US EPA, 2009. National Primary Drinking Water Regulations. https://www.epa.gov/sites/production/files/2016-06/documents/npwdr_complete_table.pdf, Accessed date: 5 December 2018.

Vanysek, Petr, 2005. Ionic conductivity and diffusion at infinite dilution. CRC Handbook of Chemistry and Physics, 84th ed CRC Press, Boca Raton.

Vörösmarty, C.J., Green, P., Salisbury, J., Lammers, R.B., 2000. Global water resources: vulnerability from climate change and population growth. Science 289, 284–288.https://doi.org/10.1126/science.289.5477.284.

Wang, H., Zhou, A., Peng, F., Yu, H., Yang, J., 2007.Mechanism study on adsorption of acidified multiwalled carbon nanotubes to Pb(II). J. Colloid Interface Sci. 316, 277–283.https://doi.org/10.1016/j.jcis.2007.07.075.

World Health Organization (Ed.), 2004. Guidelines for Drinking-Water Quality, Third. ed. World Health Organization, Geneva.

Wu, H., Liu, C., Chen, J., Yang, Y., Chen, Y., 2010. Preparation and characterization of chitosan/alpha-zirconium phosphate nanocomposite films. Polym. Int. 59, 923–930.https://doi.org/10.1002/pi.2807.

Wu, J., Zheng, Y., Song, W., Luan, J., Wen, X., Wu, Z., Chen, X., Wang, Q., Guo, S., 2014. In situ synthesis of silver-nanoparticles/bacterial cellulose composites for slowreleased antimicrobial wound dressing. Carbohydr. Polym. 102, 762–771. https://doi.org/10.1016/j.carbpol.2013.10.093.

Xiao, H., Liu, S., 2018. Zirconium phosphate (ZrP)-based functional materials: synthesis, properties and applications. Mater. Des. 155, 19–35. https://doi.org/10.1016/j.matdes.2018.05.041.

Zambelli, B., Uversky, V.N., Ciurli, S., 2016. Nickel impact on human health: an intrinsic disorder perspective. Biochim. Biophys. Acta - Proteins Proteomics 1864, 1714–1731. https://doi.org/10.1016/j.bbapap.2016.09.008.

Zhang, J., Chen, N., Su, P., Li, M., Feng, C., 2017. Fluoride removal from aqueous solution by zirconium-chitosan/graphene oxide membrane. React. Funct. Polym. 114, 127–135. https://doi.org/10.1016/j.reactfunctpolym.2017.03.008.

Zhao, D., Yu, Y., Chen, J.P., 2016. Treatment of lead contaminated water by a PVDF membrane that is modified by zirconium, phosphate and PVA. Water Res. 101, 564–573. https://doi.org/10.1016/j.watres.2016.04.078.

Zhao, H., Kwak, J.H., Conrad Zhang, Z., Brown, H.M., Arey, B.W., Holladay, J.E., 2007. Studying cellulose fiber structure by SEM, XRD, NMR and acid hydrolysis. Carbohydr. Polym. 68, 235–241. https://doi.org/10.1016/j.carbpol.2006.12.013